Tumor-Absorbed Dose for Non-Hodgkin Lymphoma Patients Treated with the Anti-CD37 Antibody Radionuclide Conjugate ^{177}Lu-Lilotomab Satetraxetan

Johan Blakkisrud[1], Ayca Løndalen[2], Anne C.T. Martinsen[1,3], Jostein Dahle[4], Jon E. Holtedahl[1], Tore Bach-Gansmo[2], Harald Holte[5], Arne Kolstad[5], and Caroline Stokke[1,6]

[1]Department of Diagnostic Physics, Oslo University Hospital, Oslo, Norway; [2]Department of Radiology and Nuclear Medicine, Oslo University Hospital, Oslo, Norway; [3]The Department of Physics, University of Oslo, Oslo, Norway; [4]Nordic Nanovector ASA, Oslo, Norway; [5]Department of Oncology, The Norwegian Radium Hospital, Oslo University Hospital, Oslo, Norway; and [6]Department of Life Science and Health, Oslo and Akershus University College of Applied Sciences, Oslo, Norway

^{177}Lu-lilotomab satetraxetan is a novel antibody radionuclide conjugate currently tested in a phase 1/2a first-in-human dosage escalation trial for patients with relapsed CD37+ indolent non-Hodgkin lymphoma. The aim of this work was to develop dosimetric methods and calculate tumor-absorbed radiation doses for patients treated with ^{177}Lu-lilotomab satetraxetan. **Methods:** Patients were treated at escalating injected activities (10, 15 and 20 MBq/kg) of ^{177}Lu-lilotomab satetraxetan and with different predosing, with or without 40 mg of unlabeled lilotomab. Eight patients were included for the tumor dosimetry study. Tumor radioactivity concentrations were calculated from SPECT acquisitions at multiple time points, and tumor masses were delineated from corresponding CT scans. Tumor-absorbed doses were then calculated using the OLINDA sphere model. To perform voxel dosimetry, the SPECT/CT data and an in-house–developed MATLAB program were combined to investigate the dose rate homogeneity. **Results:** Twenty-six tumors in 8 patients were ascribed a mean tumor-absorbed dose. Absorbed doses ranged from 75 to 794 cGy, with a median of 264 cGy across different dosage levels and different predosing. A significant correlation between the dosage level and tumor-absorbed dose was found. Twenty-one tumors were included for voxel dosimetry and parameters describing dose–volume coverage calculated. The investigation of intratumor voxel doses indicates that mean tumor dose is correlated to these parameters. **Conclusion:** Tumor-absorbed doses for patients treated with ^{177}Lu-lilotomab satetraxetan are comparable to doses reported for other radioimmunotherapy compounds. Although the intertumor variability was considerable, a correlation between tumor dose and patient dosage level was found. Our results indicate that mean dose may be used as the sole dosimetric parameter on the lesion level.

Key Words: tumor absorbed dose; antibody radionuclide conjugate; non-Hodgkin's lymphoma; dose-volume-histogram

J Nucl Med 2017; 58:48–54
DOI: 10.2967/jnumed.116.173922

Non-Hodgkin lymphoma (NHL) represents a diverse group of malignant hematologic disorders. In the United States, NHL is the fifth most common cancer, with 71,850 estimated new cases in 2015 (*1*). Most NHLs derive from B-lymphocytes and express B-cell antigens such as CD19, CD20, and CD37. Relapses are common after conventional treatments for NHL, such as external-beam radiation therapy or immunochemotherapy (*2*). Radioimmunotherapy, or antibody radionuclide conjugate (ARC) therapy, is a treatment that uses targeting antibodies linked to a radionuclide. Two ARCs are currently approved by the U.S. Food and Drug Administration: ^{131}I-tositumomab (Bexxar) and ^{90}Y-ibritumomab-tiuxetan (Zevalin) (*3*). Both agents consist of a monoclonal antibody specific for the CD20 antigen, with a β-emitting radionuclide attached. Considering that these 2 ARCs are used after patients have been treated with several rounds of rituximab, which also targets CD20, a conjugate that targets a different antigen would be desirable. ^{177}Lu-lilotomab satetraxetan (Betalutin [Nordic Nanovector ASA], previously referred to as ^{177}Lu-DOTA-HH1) is a novel ARC, in which the lilotomab antibody binds to CD37 antigens expressed on malignant B cells (*4,5*). ^{177}Lu is a β-emitter with a mean β-energy of 0.133 MeV (mean and max β-range in water, 0.25 and 1.9 mm, respectively) that also emits photons with γ-energies of 113 (6%) and 208 keV (11%), permitting γ-camera and SPECT/CT imaging as a means of dosimetry (*6*).

Insight into absorbed dose to tumors is of high importance to assess treatment efficiency. In external-beam radiation therapy, dose planning to optimize tumor dose and dose to organs at risk is considered essential. Over the last years, there has been increased focus on dosimetry also for internal emitters. Although the Committee on MIRD pamphlets suggest guidelines for normal tissue and tumor dosimetry, there is still a lack of consensus on how and when to perform dose calculations and how to evaluate doses for most radionuclide therapies. ^{131}I-tositumomab SPECT-based tumor dosimetry was initially done by daily planar imaging supported by a single SPECT acquisition (*7,8*). Later, more comprehensive dosimetric models were developed (*9*), including methods to analyze intratumor dose inhomogeneity. SPECT/CT images from multiple time points were used to obtain a predictive relationship between progression-free survival and mean tumor dose (*10,11*).

To not only evaluate the mean dose for a tumor, but also identify parts of the tumor receiving too-low doses, dose–volume

Received Feb. 7, 2016; revision accepted Jul. 5, 2016.
For correspondence or reprints contact: Caroline Stokke, The Intervention Centre, Oslo University Hospital, P.O. Box 4950 Nydalen, 0424 Oslo, Norway.
E-mail: carsto@ous-hf.no
Published online Aug. 4, 2016.

TABLE 1
Patients Included for Tumor Dosimetry

Patient no.	Sex	Dosage level (MBq/kg)	Injected activity (MBq)	Pretreatment	BSA (m^2)
2	Male	10	1,036	Rituximab + lilotomab	2.23
3	Male	10	746	Rituximab + lilotomab	1.85
5	Male	20	1,982	Rituximab + lilotomab	2.17
7	Male	20	1,505	Rituximab + lilotomab	1.86
9	Male	15	1,696	Rituximab + lilotomab	2.35
11	Male	15	1,435	Rituximab + lilotomab	2.08
13	Male	15	1,416	Rituximab	2.15
14	Female	15	1,013	Rituximab	1.68

histograms (DVHs) are routinely used in external-beam radiation therapy. Voxel-based dosimetry assigning each voxel an absorbed dose is the foundation for creating DVHs. To do this accurately requires tracking of the radioactivity in each voxel over time, which, for tumors subjected to deformation, can be a challenging task. A dose–rate–volume histogram will instead depict the dose rates in a tumor at an instant moment.

The aim of the current work was to develop dosimetric procedures and establish tumor-absorbed doses for patients in the phase 1 study of ^{177}Lu-lilotomab satetraxetan, both on a mean tumor and on a tumor voxel level.

MATERIALS AND METHODS

Patient Population and Treatment

Eight patients with relapsed indolent NHL treated in the phase 1 LYMRIT-37-01 trial were included for tumor dosimetry. This study was approved by the regional ethical committee, and all patients had signed an informed consent form. The participants received a single injection of ^{177}Lu-lilotomab satetraxetan. To deplete normal B cells, 2 infusions of rituximab (375 mg/m^2) were given at 4 and 3 wk before administration of ^{177}Lu-lilotomab satetraxetan. In addition, 2 different predosing regimes were tested; patients in arm 1 were predosed with 40 mg of unlabeled antibody (lilotomab) 4 h before injection, and patients in arm 2 were not. ^{177}Lu-lilotomab satetraxetan was administered at a fixed amount of activity per body weight (dosage level), ranging from 10 to 20 MBq/kg (Table 1). Body surface area (BSA) was calculated using the Dubois and Dubois method (*12*).

Image Acquisition and Reconstruction

All patients were imaged using a dual-head Symbia T16 SPECT/CT scanner (Siemens), equipped with a 0.952-cm (0.375-in)-thick NaI crystal and a medium-energy collimator. Patients in arm 1 underwent 2 SPECT/CT scans at 96 and 168 h after ^{177}Lu-lilotomab satetraxetan. Patients in arm 2 underwent 3 SPECT/CT scans at after 24, 96, and 168 h. Figure 1 shows SPECT/CT images for 1 of the patients. Energy windows were centered at the 113- and 208-keV photon peaks with 20% window width. Two lower scatter windows with a 20% width were used. Scans were obtained with 2 × 32 projections, each of 45-s frame length in a noncircular orbit in step-and-shoot mode. Attenuation and scatter corrections were performed using the vendor's software (Siemens Medical Esoft). An ordered-subset expectation maximization reconstruction was used, having 4 iterations and 16 subsets and a gaussian filtration of 4 mm. The matrix size was 128 × 128, with a pixel size of 4.8 mm. Collimator compensation was not used. CT scans were acquired with 30 mAs and 130-keV tube voltage. The matrix size was 512 × 512, with 3-mm slice thickness.

Scanner Calibration and Phantom Measurements

SPECT/CT data were analyzed using the software program PMOD (version 3.6; PMOD Industries). A calibration factor was found using an anthropomorphic Torso Model ECT/TOR/P water-filled phantom (Data Spectrum Corp.) containing an insertion with 106.3 MBq of ^{177}Lu-lilotomab satetraxetan in 1.2 L of water. Resolution was measured by a capillary tube. A series of phantom measurements with spheric insertions (2, 4, 8, 16, and 113 mL) was also performed. Initial activity concentration in the spheres was 0.69 MBq/mL, with subsequent activity concentrations being 0.37, 0.13, and 0.03 MBq/mL. Volumes of interest (VOIs) were drawn with 10- and 20-mm margins around the sphere walls. In addition, manually defined VOIs were drawn to include all counts seemingly originating from the spheres.

Lesion Delineation

Twenty-six tumors were included. Lesions were included on the basis of the following criteria: visual identification of lesion on CT and activity on SPECT as well as a minimum volume of 1.5 mL. Delineation was primarily performed on the scan performed at 96 h. Two individual VOIs were defined for each tumor, both drawn manually in a slice-by-slice

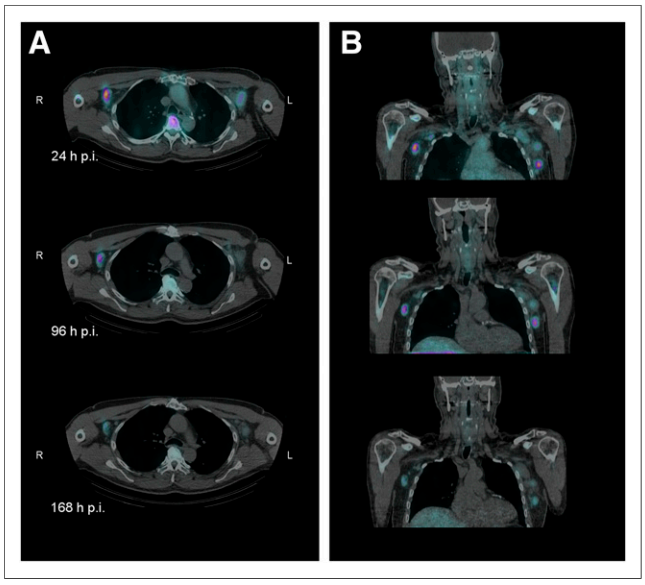

FIGURE 1. Axial (A) and coronal (B) SPECT/CT-fused images of patient 13 at 3 time points after administration of ^{177}Lu-lilotomab satetraxetan. Tumor 13b can be seen in left axilla and 13c in the right. Tumor dosimetry was based on multiple SPECT/CT scans. p.i. = after injection.

manner by an experienced nuclear medicine specialist. An anatomic VOI, VOI_{CT}, was drawn tangent to the tumor edge. A functional VOI, VOI_{SPECT}, was drawn on the SPECT image with a manually defined margin. These 2 VOIs were then transferred to the 168- and 24-h datasets.

Dose Calculation

The counts in VOI_{SPECT} were converted to activity. A time–activity curve was calculated from 2 time points (3 in arm 2 for comparison) by assuming a monoexponential clearance with an effective half-life t_{eff}. Following the MIRD formalism, the total number of disintegrations is:

$$\tilde{A} = \int_0^\infty A_0 e^{-\frac{ln(2)}{t_{eff}}t} dt.$$

Absorbed dose is then calculated by

$$\overline{D} = \frac{\tilde{A}}{m_{CT}} \overline{S},$$

where m_{CT} is the tumor mass, found by the volume of VOI_{CT} and assuming uniform mass density equal to water. $\overline{S}$ is a dose factor of 8.56 10^{-5} Gykg/MBqh calculated from the OLINDA/EXM uniform density sphere model for a sphere of 10 g (*13*). The error of $\overline{S}$ for the tumor volumes in this work is about 1%. To compare doses across dosage levels, $\overline{D}$ was normalized by administered activity.

Voxel Dosimetry

The voxel dosimetry was performed by the local deposition method (*14*). Tumors larger than 4 mL were included for voxel dosimetry, 21 tumors in total. SPECT data and the anatomic VOI were exported from PMOD and analyzed using in-house–developed software written in MATLAB (version 2015a; The MathWorks Inc.). The SPECT activity data were multiplied with a dose conversion constant, based on the assumption of 0.133 MeV of energy absorbed per disintegration. The dose rate maps were further analyzed by constructing cumulative dose–rate–volume histograms (cDRVHs).

Statistics

A Mann–Whitney *U* test was performed to investigate whether tumor doses for arm 1 and arm 2 differed. A null-hypothesis of equal populations with a rejection level of 0.05 was set. The relationship between mean absorbed dose and the following parameters was investigated for tumors belonging to patients in arm 1: activity per body weight (dosage level), total administered activity, activity per BSA,

TABLE 2
Tumor Characteristics and Mean Tumor-Absorbed Doses

Tumor	Localization	Tumor mass (g)	Effective half-life (days)	Dose (cGy)	Dose/injected activity (mGy/MBq)
2a	Neck, right lower	6.2	2.9	151	1.5
2b	Neck, right upper	9.8	3.0	87	0.8
2c	Paraesophageal	9.4	5.4	75	0.7
3a	Paratracheal, right	6.2	4.7	201	2.7
3b	Neck, left lower	1.8	8.1	90	1.2
3c	Paravertebral, right	14.9	3.3	282	3.8
5a	Inguinal, right	12.5	3.4	207	1.0
5b	Subcut nates, right	25.0	3.7	90	0.5
5c	Retroperitoneum	8.1	4.0	327	1.6
7a	Inguinal, left middle	10.9	4.2	794	5.3
7b	Inguinal, left upper	18.0	3.3	550	3.7
7c	Inguinal, right	3.2	3.8	359	2.4
7d	Inguinal, left lower	22.5	3.3	320	2.1
9a	Mediastinum, anterior	14.4	4.2	328	1.9
9b	Inguinal, right	5.0	3.2	204	1.2
9c	Mediastinum, right upper	15.5	2.0	130	0.8
11a	Axilla, left	2.3	4.2	672	4.7
11b	Neck, right	4.4	3.1	277	1.9
11c	Inguinal, left	1.5	3.9	422	2.9
Mean values arm 1		10.1			2.1
13a	Axilla, left lower	15.7	2.0	268	1.9
13b	Axilla, left upper	15.6	2.5	123	0.9
13c	Axilla, right lower	14.5	2.4	728	5.1
13d	Axilla, right upper	4.3	2.9	139	1.0
14a	Inguinal, right	3.8	2.7	245	2.4
14b	Inguinal, left lower	6.4	2.6	259	2.5
14c	Inguinal, left upper	7.2	3.1	338	3.3
Mean values arm 2		9.6			2.5

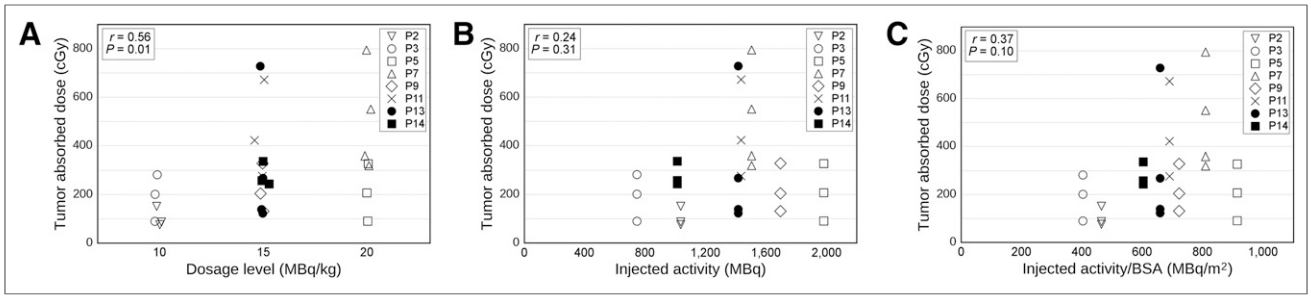

FIGURE 2. Tumor-absorbed dose related to several parameters. Each symbol represents a tumor, and filled and open symbols represent arms 1 and 2, respectively. (A) Absorbed doses versus administered activity normalized by body weight (dosage level). Patients in this study were treated according to this dosage method. (B) Absorbed dose versus total administered activity. (C) Absorbed dose versus administered activity normalized by BSA. The latter 2 (B and C) represent hypothetic dosage regimes.

and tumor mass. The Spearman rank correlation coefficient with a significance level of P less than 0.05 was used. The relationship between mean dose and dose rate covering the 10%, 50%, and 90% of the tumor volume ($D_{10\%}$, $D_{50\%}$, and $D_{90\%}$, respectively) for both arms 1 and 2 was investigated using the Spearman rank test. All statistical calculations were conducted using MATLAB version 2015a.

RESULTS

Phantom Studies and Margin-Based Quantification Method

The calibration factor was 15.9 Bq/counts, and the full width at half maximum was 19.2 mm. The results of the phantom acquisitions are found in Supplemental Table 1 (supplemental materials are available at http://jnm.snmjournals.org). A 10-mm margin generally led to an underestimation of activity and 20 mm to an overestimation. The latter was due to contribution from the surrounding spheres. Mean errors for manually defined margins, the quantification method used for the patient tumors, ranged from −3.5 to −1.3%.

Mean Tumor-Absorbed Doses

Twenty-six tumors from 8 patients were included for dosimetry (Table 2). Interpatient variations were observed, with tumor-absorbed doses ranging from 75 to 794 cGy across different dosage levels. For patients included in arm 1, the mean overall tumor-absorbed dose was 2.1 mGy/MBq (range, 0.5–5.3 mGy/MBq). The patients in arm 2 received a mean overall tumor-absorbed dose of 2.5 mGy/MBq (range, 0.9–5.1 mGy/MBq). There was no statistically significant difference between doses in arms 1 and 2 ($P = 0.60$), indicating that the 40-mg predosing did not change the tumor uptake of ^{177}Lu-lilotomab satetraxetan. For patients in the 10 MBq/kg group, 15 MBq/kg group, and 20 MBq/kg group in arm 1, the median dose was 120, 302, and 327 cGy, respectively. For patients in the 15 MBq/kg group in arm 2, the median dose was 259 cGy.

The tumor-absorbed dose increased significantly with the administered activity divided by body weight (dosage level) in arm 1 (Fig. 2A). In contrast, the tumor-absorbed dose did not increase with total injected activity (Fig. 2B). Figure 2C shows tumor-absorbed dose plotted against administered activity divided by BSA. The tumor mass varied, with an average of 10.0 g (Table 2). There was no statistically significant relationship between tumor-absorbed dose and tumor mass (Fig. 3).

The largest intrapatient variation in arm 1 in absolute dose values was found in patient 7, displaying tumor-absorbed doses ranging from 320 to 794 cGy. Patient 13 displayed the largest variation in arm 2. For all patients in arm 1, the intrapatient dose ratio (the ratio between the highest and lowest tumor dose in the patient) was larger than 2:1. For 3 of 6 patients, the same ratio was larger than 2.5:1.

Dose–Rate–Volume Histograms

Figure 4 illustrates a dose rate map and the accompanying cDRVH for tumor 5b. The cDRVHs for all tumors included are shown in Figure 5. The cDRVHs differ somewhat in shape. For example, tumor 5c shows a long plateau and a steep fall down to zero, indicating a fairly homogeneous dose. In contrast, tumor 5a has a more gradual decrease, indicating a larger spread in dose rates in different parts of the tumor.

Table 3 quantifies the shape of cDRVH. The $D_{10\%}$, $D_{50\%}$, and $D_{90\%}$ are shown. A strong correlation was found between mean-absorbed dose and the dose rate thresholds $D_{10\%}$ ($r = 0.77$ $P < 0.0001$), $D_{50\%}$ ($r = 0.82$ $P < 0.0001$), and $D_{90\%}$ ($r = 0.58$ $P = 0.006$).

DISCUSSION

Knowledge about tumor-absorbed dose is fundamental for the evaluation of new ARC treatments. Here, we have calculated both mean tumor dose and dose rate on the voxel level for a first-in-human study of ^{177}Lu-lilotomab satetraxetan.

The median dose across the patient population was 264 cGy. Even though lymphomas are radiation sensitive, this can be

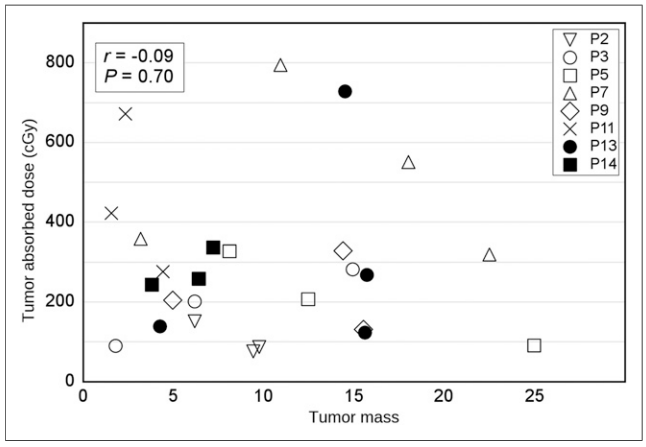

FIGURE 3. Tumor-absorbed dose plotted against individual tumor mass. Filled and open symbols represent tumors belonging to patients in arms 1 and 2, respectively. Interestingly, no correlation was found between absorbed dose and tumor mass.

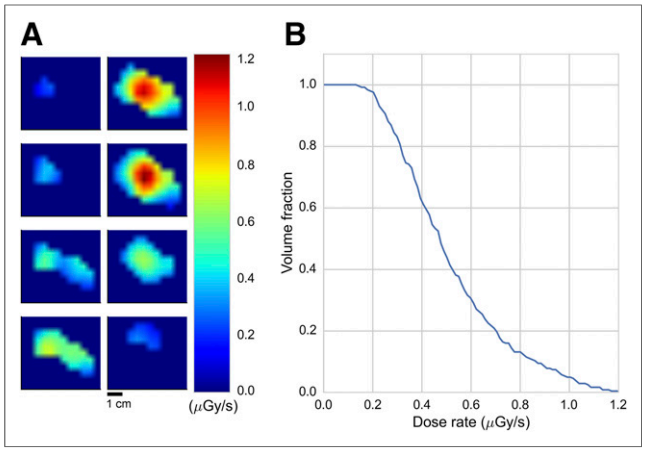

FIGURE 4. (A) Voxel dose rate map illustrated for tumor 5b, a subcutaneous tumor residing in right nates area of patient 5. Eight axial slices show tumor volume superior to inferior. Color bar indicates dose rate of different voxels. (B) Corresponding cDRVH shows dose rate to different volume fractions of tumor, for example, a dose rate of about 0.5 μGy/s covers half of the tumor.

considered a relatively low radiation dose compared with doses in external-beam radiation therapy (*15*). However, for other ARCs absorbed doses of the same order of magnitude as the doses found here have been reported. For ^{131}I-tositumomab, the tumor doses have ranged from 102 to 711 cGy (*16*). In a study that correlated tumor-absorbed dose and progression-free survival for ^{131}I-tositumomab treatment, a significant difference in progression-free survival was observed when a dose threshold of 200 cGy was used (*11*). This 200-cGy threshold is slightly below the estimated median dose delivered to patients in our study. Tumor dose estimates for ^{90}Y-ibritumomab-tiuxetan were found in the range of 580–6,700 cGy in 1 study (*17*). There is more uncertainty around these data, because the dosimetry was based on planar imaging of a substitute ligand with the radionuclide ^{111}In. However, the concept of absorbed dose by itself is not suitable for comparing external and internal radiation therapy or even internal emitters loaded with different radionuclides. The differences in both physical and biologic parameters make direct evaluation of both tumor and normal tissue–absorbed doses for ^{177}Lu-lilotomab satetraxetan somewhat challenging. Still, our results indicate that red marrow–absorbed doses can be kept below 200 cGy with the above-mentioned tumor-absorbed doses (*18*).

Correlation of tumor-absorbed dose and patient dosage level demonstrated a significant increase in tumor dose for increasing dosage level (Fig. 2A). This increase indicates that the chosen dosage regime ensures higher tumor dose for increasing levels of activity per body weight, regardless of patient shape. We also investigated whether other dosage regimes could demonstrate better prediction of tumor dose. Dosage with a fixed activity is known from treatment of, for example, thyroid cancer (*19*) and dosage determined by BSA adjusted activity from a study of ^{177}Lu-DOTA-rituximab (*20*). However, our results indicate that these 2 other theoretic regimes would not deliver higher tumor-absorbed doses if the patient dosage was increased. Although the current dosage method (activity/body weight) seems the best suited, a rather low *r* value of 0.56 for the tumor dose and patient dosage level correlation may suggest that there are more optimal means for delivering this treatment.

Intrapatient variability in absorbed tumor dose was observed, most striking in patient 13. This patient had both the minimum and the maximum tumor-absorbed dose in the 15 MBq/kg groups considering both arm 1 and 2. Interestingly, these 2 tumors had almost identical size and were both located in the axillary area contralaterally (Fig. 1). A possible explanation for the intrapatient variability could be differences in expression of the target antigen CD37. Another explanation may be different vascularization, but the lack of correlation between tumor dose and mass in our study contradicts this hypothesis (Fig. 3).

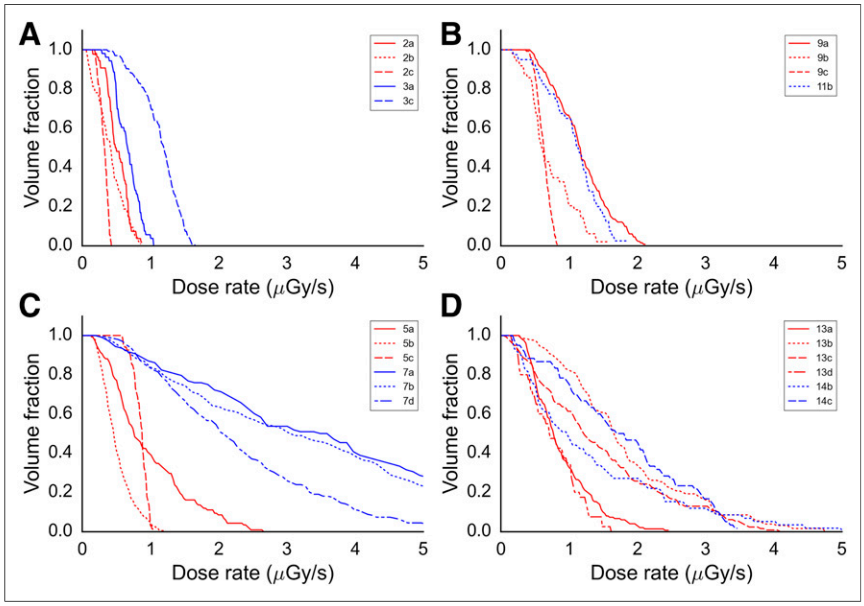

FIGURE 5. cDRVHs of individual tumors included for voxel dosimetry. Histograms show minimum dose rate to different fractions of tumor volumes. Tumors are grouped by dosage level: 10, 15, and 20 MBq/kg for arm 1 and 15 MBq/kg for arm 2 in A, B, C, and D, respectively. The 2 colors in each panel represent 2 patients included at each dosage level. Absolute size and position of each tumor can be found in Table 2 and dose rates in Table 3.

In this study, quantification of radioactivity uptake has been investigated using spheres imitating lesions and larger margin-based VOIs to allow for spill-out effects of the imaging system and patient motion during the long acquisitions. The results indicate a well-functioning quantification routine and are similar to previous results for ^{177}Lu (*21*). Quantification can alternatively be performed by the use of recovery coefficients. This scheme is often chosen for quantification of ^{131}I because the energy of this nuclide is higher (*22*) but has also been found suited for ^{177}Lu peptide receptor radionuclide therapy (*23*). Because we have much lower activity concentration and virtually no background activity, the large VOI method was here preferred to allow some blurring due to patient motion. Mono-exponential activity clearance is an approximation that has been used under similar conditions (*24–26*). The limited number of data points for the tumors belonging to

TABLE 3
Minimum Dose Rates Covering 10%, 50%, and 90% of Tumor Volumes

Tumor	$\dot{D}_{10\%}$ (μGy/s)	$\dot{D}_{50\%}$ (μGy/s)	$\dot{D}_{90\%}$ (μGy/s)
2a	0.7	0.5	0.3
2b	0.7	0.4	0.1
2c	0.4	0.3	0.2
3a	0.9	0.7	0.5
3c	1.5	1.2	0.7
5a	1.9	0.8	0.3
5b	0.9	0.5	0.3
5c	1.0	0.9	0.7
7a	7.1	3.7	0.9
7b	6.8	3.1	0.8
7d	4.1	2.1	0.9
9a	1.8	1.2	0.6
9b	1.3	0.6	0.3
9c	0.8	0.6	0.5
11b	1.6	1.2	0.6
13a	1.5	0.8	0.4
13b	3.1	1.7	0.8
13c	3.2	1.2	0.3
13d	1.3	0.7	0.3
14b	3.2	1.0	0.3
14c	3.2	1.8	0.4

patients in arm 1 can introduce uncertainty for the time–activity curves. Patients in arm 2 were scanned 3 times, potentially improving this factor. Although the calculated dose using 2 or 3 time points for these patients was found having a mean error of 5.5% ($n = 7$, maximum error 16%, data not shown), fit-related parameters probably introduce the larger uncertainty of this study. The mean tumor dose calculation takes into account the contribution from radiation inside the tumor, neglecting cross fire from surrounding tissue. Use of the OLINDA-unit-sphere model for tumors has been compared with a full Monte Carlo simulation for ^{131}I (*16*). An excellent agreement for self-dose, and good agreement when cross fire was included, was then found. Because ^{177}Lu has both shorter path lengths of the electrons and considerably less cross fire, an even better agreement is assumed.

To accurately determine DVHs, activity of the individual voxels must be tracked between multiple time points, in analog to the time–activity curve used in the mean tumor-absorbed dose model. Temporal tracking has been investigated by radial deformations of tumors (*10*). Our dose rate maps only depict the doses at day 4, and although not providing the complete dosimetric picture, they are neither prone to mismatched registration of maps from different time points. Another method for voxel dosimetry has been based on calculation of the voxel dose rates at a single time point and assumption of the same activity washout for each voxel as for the whole tumor (*27*). Combining the cDRVHs (Fig. 5) and the effective half-lives (Table 2) here provides analog information. The shape of the cDVHs would remain exactly the same as the cDRVHs and all statistical correlations between mean dose and $D_{xx\%}$ identical.

Our analysis of the dose rate maps suggests that inter- and intratumor variability exist on the voxel level. Although mean absorbed dose values can be useful, knowledge of how this dose is distributed must be considered before meaningful interpretations can be made. This is especially important for response evaluation; a high mean dose can be found whereas parts of the tumor still receive zero absorbed dose. Here, a strong monotonic relationship has been found between the dose rates covering 50% and 10% of the volume and the mean absorbed doses (Table 3). If the mean dose value is predictive of the other dose–volume parameters, these comprehensive voxel analyses are perhaps redundant.

CONCLUSION

Dosimetric methods following the MIRD formalism for internal emitters have been developed on 2 levels, for whole tumors considering the mean absorbed dose and on a voxel-level using cDRVHs. The methods correlate with each other, indicating that one of them could be rendered redundant. Tumor-absorbed doses increase with dosage level for patients treated with ^{177}Lu-lilotomab satetraxetan and are comparable to other ARCs.

DISCLOSURE

This study was sponsored by Nordic Nanovector ASA. Johan Blakkisrud was in part supported by grants from Nordic Nanovector ASA. Harald Holte and Arne Kolstad were both in part supported by grants from the Norwegian Cancer Society. No other potential conflict of interest relevant to this article was reported.

ACKNOWLEDGMENTS

We thank the personnel at the Nuclear Medicine section at Oslo University Hospital for technical assistance with the acquisitions. Stine Nygaard, study nurse at the Department of Oncology, is also greatly acknowledged. In addition, we thank the anonymous reviewers for their suggestions.

REFERENCES

1. Siegel RL, Miller KD, Jemal A. Cancer statistics, 2015. *CA Cancer J Clin.* 2015;65:5–29.
2. Chao MP. Treatment challenges in the management of relapsed or refractory non-Hodgkin's lymphoma: novel and emerging therapies. *Cancer Manag Res.* 2013;5:251–269.
3. Jacene HA, Filice R, Kasecamp W, Wahl RL. Comparison of ^{90}Y-ibritumomab tiuxetan and ^{131}I-tositumomab in clinical practice. *J Nucl Med.* 2007;48:1767–1776.
4. Repetto-Llamazares AHV, Larsen RH, Patzke S, et al. Targeted cancer therapy with a novel anti-CD37 beta-particle emitting radioimmunoconjugate for treatment of non-Hodgkin lymphoma. *PLoS One.* 2015;10:e0128816.
5. Smeland E, Funderud S, Ruud E, Kiil Blomhoff H, Godal T. Characterization of two murine monoclonal antibodies reactive with human B cells: their use in a high-yield, high-purity method for isolation of B cells and utilization of such cells in an assay for B-cell stimulating factor. *Scand J Immunol.* 1985;21:205–214.
6. Jødal L. Beta emitters and radiation protection. *Acta Oncol.* 2009;48:308–313.
7. Koral KF, Dewaraja Y, Li J, et al. Initial results for hybrid SPECT-conjugate-view tumor dosimetry in ^{131}I-anti-B1 antibody therapy of previously untreated patients with lymphoma. *J Nucl Med.* 2000;41:1579–1586.
8. Koral KF, Dewaraja Y, Li J, et al. Update on hybrid conjugate-view SPECT tumor dosimetry and response in ^{131}I-tositumomab therapy of previously untreated lymphoma patients. *J Nucl Med.* 2003;44:457–464.
9. Sgouros G, Frey E, Wahl R, He B, Prideaux A, Hobbs R. 3-D imaging based, radiobiological dosimetry. *Semin Nucl Med.* 2008;38:321–334.

10. Dewaraja YK, Schipper MJ, Roberson PL, et al. ^{131}I-tositumomab radioimmunotherapy: initial tumor dose–response results using 3-dimensional dosimetry including radiobiologic modeling. *J Nucl Med.* 2010;51:1155–1162.
11. Dewaraja YK, Schipper MJ, Shen J, et al. Tumor-absorbed dose predicts progression-free survival following ^{131}I-tositumomab radioimmunotherapy. *J Nucl Med.* 2014;55:1047–1053.
12. Bois D, Bois E. Clinical calorimetry: tenth paper—a formula to estimate the approximate surface area if height and weight be known. *Arch Intern Med (Chic).* 1916;17:863–871.
13. Stabin MG, Konijnenberg MW. Re-evaluation of absorbed fractions for photons and electrons in spheres of various sizes. *J Nucl Med.* 2000;41:149–160.
14. Pasciak AS, Bourgeois AC, Bradley YC. A comparison of techniques for ^{90}Y PET/CT image-based dosimetry following radioembolization with resin microspheres. *Front Oncol.* 2014;4:121.
15. Lowry L, Smith P, Qian W, et al. Reduced dose radiotherapy for local control in non-Hodgkin lymphoma: a randomised phase III trial. *Radiother Oncol.* 2011;100:86–92.
16. Howard DM, Kearfott KJ, Wilderman SJ, Dewaraja YK. Comparison of I-131 radioimmunotherapy tumor dosimetry: unit density sphere model versus patient-specific Monte Carlo calculations. *Cancer Biother Radiopharm.* 2011;26:615–621.
17. Wiseman GA, White CA, Stabin M, et al. Phase I/II ^{90}Y-zevalin (yttrium-90 ibritumomab tiuxetan, IDEC-Y2B8) radioimmunotherapy dosimetry results in relapsed or refractory non-Hodgkin's lymphoma. *Eur J Nucl Med.* 2000;27:766–777.
18. Blakkisrud J, Løndalen A, Dahle J, et al. Red marrow absorbed dose for non-Hodgkin lymphoma patients treated with ^{177}Lu-lilotomab satetraxetan, a novel anti-CD37 antibody radionuclide conjugate. *J Nucl Med.* September 1, 2016 [Epub ahead of print].
19. Freitas JE, Gross MD, Ripley S, Shapiro B. Radionuclide diagnosis and therapy of thyroid cancer: current status report. *Semin Nucl Med.* 1985;15:106–131.
20. Forrer F, Oechslin-Oberholzer C, Campana B, et al. Radioimmunotherapy with ^{177}Lu-DOTA-rituximab: final results of a phase I/II study in 31 patients with relapsing follicular, mantle cell, and other indolent B-cell lymphomas. *J Nucl Med.* 2013;54:1045–1052.
21. Beauregard J-M, Hofman MS, Pereira JM, Eu P, Hicks RJ. Quantitative ^{177}Lu SPECT (QSPECT) imaging using a commercially available SPECT/CT system. *Cancer Imaging.* 2011;11:56–66.
22. Dewaraja YK, Frey EC, Sgouros G, et al. MIRD pamphlet no. 23: quantitative SPECT for patient-specific 3-dimensional dosimetry in internal radionuclide therapy. *J Nucl Med.* 2012;53:1310–1325.
23. Ilan E, Sandström M, Wassberg C, et al. Dose response of pancreatic neuroendocrine tumors treated with peptide receptor radionuclide therapy using ^{177}Lu-DOTATATE. *J Nucl Med.* 2015;56:177–182.
24. DeNardo DA, DeNardo GL, Yuan A, et al. Prediction of radiation doses from therapy using tracer studies with iodine-131-labeled antibodies. *J Nucl Med.* 1996;37:1970–1975.
25. Buckley SE, Saran FH, Gaze MN, et al. Dosimetry for fractionated ^{131}I-mIBG therapies in patients with primary resistant high-risk neuroblastoma: preliminary results. *Cancer Biother Radiopharm.* 2007;22:105–112.
26. Sandström M, Garske U, Granberg D, Sundin A, Lundqvist H. Individualized dosimetry in patients undergoing therapy with ^{177}Lu-DOTA-D-Phe1-Tyr3-octreotate. *Eur J Nucl Med Mol Imaging.* 2010;37:212–225.
27. Sgouros G, Squeri S, Ballangrud ÅM, et al. Patient-specific, 3-dimensional dosimetry in non-Hodgkin's lymphoma patients treated with ^{131}I-anti-B1 antibody: assessment of tumor dose-response. *J Nucl Med.* 2003;44:260–268.